International Journal of Biological Macromolecules 261 (2024) 129870

Contents lists available at ScienceDirect

International Journal of Biological Macromolecules

journal homepage: www.elsevier.com/locate/ijbiomac

Mining and tailor-made engineering of a novel keto reductase for asymmetric synthesis of structurally hindered γ- and δ-lactones

Shuo Wang, Guochao Xu *, Ye Ni *

Key laboratory of industrial Biotechnology, Ministry of Education, School of Biotechnology, Jiangnan University, Wuxi 214122, Jiangsu, China

ARTICLE INFO

Keywords:
Carbonyl reductase
Long-chain aliphatic keto acid
(*S*)-Lactones
Structurally hindered substrate
Tailor-made engineering

ABSTRACT

A novel carbonyl reductase from *Hyphopichia burtoni* (*Hb*KR) was discovered by gene mining. *Hb*KR is a NADPH-dependent dual function enzyme with reduction and oxidation activity belonging to SDR superfamily. *Hb*KR strictly follows Prelog priority in the reduction of long-chain aliphatic keto acids/esters containing remote carbonyl groups, such as 4-oxodecanoic acid and 5-oxodecanoic acid, producing (*S*)-γ-decalactone and (*S*)-δ-decalactone in >99 % *e.e.* Tailor-made engineering of *Hb*KR was conducted to improve its catalytic efficiency. Variant F207A/F86M was obtained with specific activity of 8.37 U/mg toward 5-oxodecanoic acid, which was 9.7-fold of its parent. Employing F207A/F86M, 100 mM 5-oxodecanoic acid could be reduced into optically pure (*S*)-δ-decalactone. Molecular docking analysis indicates that substitution of aromatic Phe with smaller residues renders sufficient space for accommodating substrates in a more stable conformation. This study offers an efficient biocatalyst for the biosynthesis of (*S*)-lactones, and provides guidance for engineering carbonyl reductases toward structurally hindered substrates.

1. Introduction

Chiral aliphatic γ- and δ-lactone and their derivatives are the key chiral building blocks of many natural products and drugs [1]. For example, the γ- and δ-decalactone obtained by the cyclization of γ- and δ-hydroxy acids/esters are flavors and fragrances widely used in the food industry [2]. The difference in the chiral configuration of the chemical structure makes the different fragrance characteristics [3]. The aroma of spices and fragrances is perceived by organisms through enzymes or receptor molecules on the surface of cells, so the aroma characteristics and intensity of fragrance compounds are closely related to their space structure [4]. According to literature, the fragrance of (*R*)-γ-and δ-decalactone is relatively stronger, while the fragrance of (*S*)-γ-and δ-decalactone is softer [5]. These lactones find a variety of commercial uses within flavourings and fragrances, in particular δ-decalactone, a common fragrance compound, with the (*S*)-enantiomer presenting a significantly more intense creamy peach note compared to the (*R*)-isomer, which is found preferentially in nature [6]. In addition, γ-decalactone is also very important in flavor applications with a global market volume of several hundred tons per year [7]. (*R*)-γ-decalactone has an aroma of coconut, fruity-fatty, while (*S*)-γ-decalactone features a softer aroma of coconut, caramel, fatty and fruit [8]. In addition to the stereo-configuration of the aroma compound, the aroma characteristics are usually affected by the molecular size, functional groups, shape and volatility [9]. Compared with racemic lactones, chiral lactones often feature purer flavor characteristics. Moreover, different fragrance characteristics can be obtained by adjusting composition ratio of the (*R*) and (*S*) types [10]. Specific and characteristic enantiomeric ratios have been reported for lactones in apricots, peaches, raspberries, strawberries, plums, mangos, and passionfruit and juices, wines, and spirits [11]. Interestingly, γ-and δ-decalactone has a wide range of antibacterial activities. For example, γ-and δ-decalactone had been reported to inhibit the growth of selected filamentous fungi (*Aspergillus niger* etc), yeasts (*Candida albicans* etc) and bacteria (*Staphylococcus aureus* etc). The inhibitory activities of lactone enantiomers are different. Compared with (*R*)-γ-decalactone, (*S*)-γ-decalactone showed more durable effect for at least 24 h [12].

Recently, Arai et al. synthesized chiral aromatic lactones and diols using a ruthenium catalyst by changing the reaction conditions (Scheme 1a) [13]. Meninno et al. developed organometallic catalyst quinine for chiral ketone ester compounds (Scheme 1b) [14]. Oscar et al. performed kinetic resolution of racemic δ-hydroxy esters via lipase-catalyzed transesterification, combining enzymatic kinetic resolution with ruthenium-catalyzed alcohol racemization (Scheme 1c) [15]. Although

* Corresponding authors.
E-mail addresses: guochaoxu@jiangnan.edu.cn (G. Xu), yni@jiangnan.edu.cn (Y. Ni).

https://doi.org/10.1016/j.ijbiomac.2024.129870
Received 7 November 2023; Received in revised form 25 January 2024; Accepted 29 January 2024
Available online 30 January 2024

noble metal and organometallic catalysis is an effective method for stereoselective synthesis of hydroxyl esters, this method requires harsh reaction conditions, such as pressure, temperature etc., and particularly, is not environmentally friendly. Biocatalytic synthesis of optically active γ- and δ-decalactone for applications in food and cosmetics industry, is drawing increasing attentions. Compared with chemical catalysis methods, biocatalysis methods have a number of advantages such as high stereoselectivity, mild conditions, lower cost etc. [16].

Many short-chain and poly-substituted lactones have been synthesized by enzymatic reductions of γ-/δ-keto acids/esters. Chu et al. isolated a novel alkene reductase (*Ss*ER) from *Swingsia samuiensis*, combined with carbonyl reductase *Ss*CR to synthesize optically pure tobacco lactones and whisky lactones from α, β-unsaturated γ-ketone esters [17]. However, the stereoselective reduction of long-chain alkyl γ-/δ-keto acids/esters remains challenging because of the bulky carbon chain and remote position of the carbonyl group. Recently, Xu and coworkers discovered a carbonyl reductase *Sm*CR from *Serratia marcescens* that can asymmetrically catalyze the reduction of long-chain aliphatic γ- and δ-keto acids/esters to produce corresponding γ- and δ-lactones [18]. (*R*)-γ-decalactone and (*R*)-δ-decalactone were synthesized by *Sm*CR in 99 % *e.e.* and 95 % *e.e.,* respectively. However, the activity of *Sm*CR was not sufficient for practical application. Subsequently, *Sm*CR was engineered with greatly improved catalytic properties (Scheme 1d) [19]. Importantly, enzymatic reduction approach is more atomically economical compared with biocatalytic resolution. However, there are few reports on the bioreductive synthesis of (*S*)-lactones. Recently, Özgen and coworkers developed the synthesis of a (*S*)-γ-lactones based on combined photocatalysis and biocatalysis [20], in which tetrabutylammonium decatungstate was employed as the photocatalyst to trigger the hydroacylation of starting olefins, to produce keto esters/acids, followed by synthesis of chiral alcohols catalyzed by ADH.

To develop an enzymatic approach for synthesizing (*S*)-lactones, gene mining and tailor-made engineering of carbonyl reductase were performed in this work. Using carbonyl reductase *Cp*AR2 from *Candida parapsilosis* as probe, a novel and *S*-stereoselective keto reductase *Hb*KR from *Hyphopichia burtoni* was identified. The catalytic efficiency of *Hb*KR was further engineered for the synthesis of (*S*)-γ and δ-decalactones (Scheme 1e). Various oxocarboxylic acids and esters with high structural hindrance were also reduced asymmetrically.

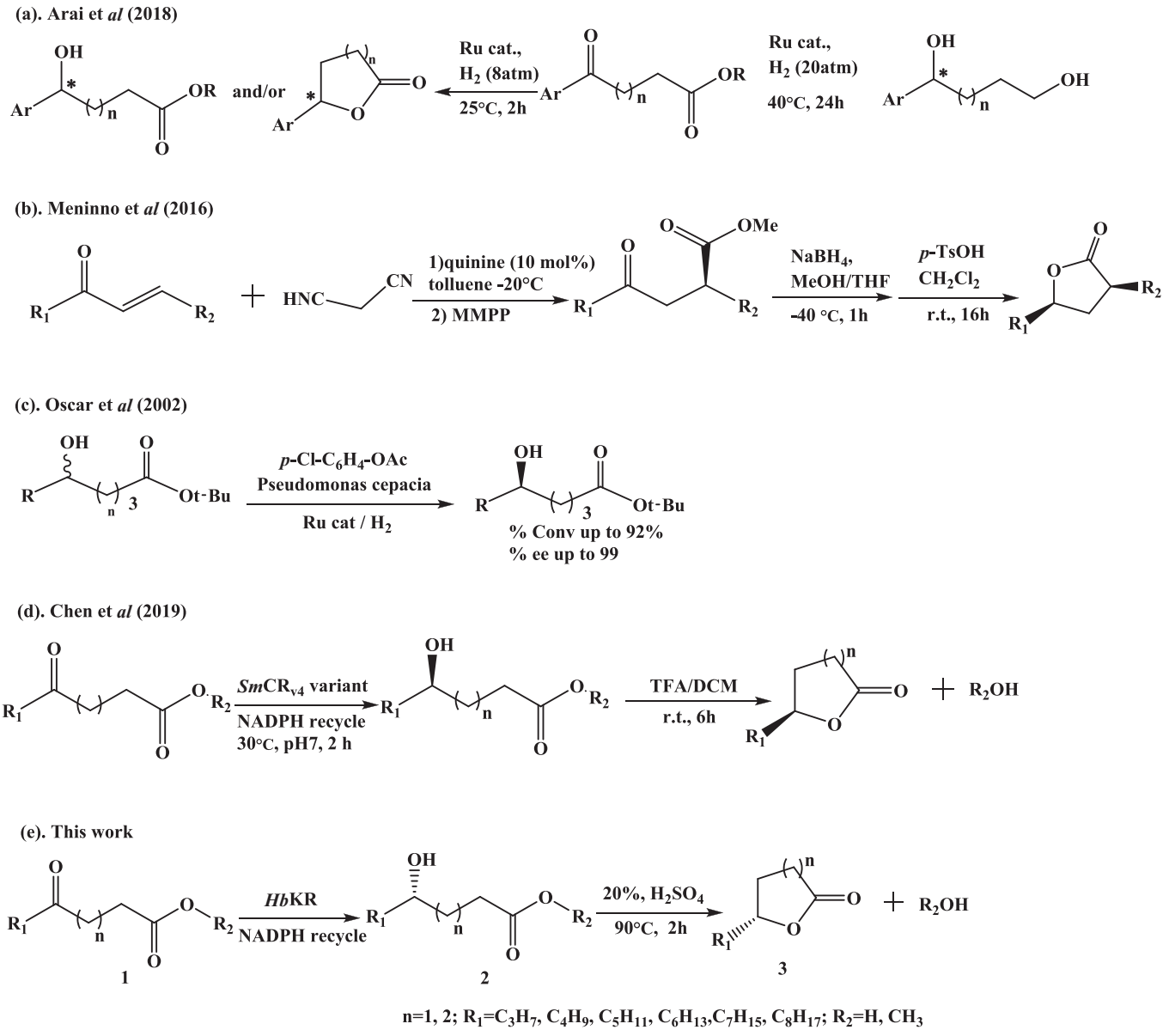

Scheme 1. Stereoselective synthesis of optically pure γ- and δ-lactones in this work and literatures.

2. Materials and methods

2.1. Chemical reagents

Racemic γ-decalactone, δ-decalactone were obtained from Aladdin. γ-Caprolactone, δ-caprolactone, γ-dodecalactone, δ-dodecalactone and N-bromosuccinimide Amine (NBS) were purchased from Macklin.

2.2. Synthesis of 4-oxodecanoic acid, 4-oxodecanoic acid methyl ester, 5-oxodecanoic acid, 5-oxodecanoic acid methyl ester

Using NBS as oxidation catalyst, racemic γ or δ-decalactone was converted into 4 or 5-oxodecanoic acid. In 20 mL water, 5 mmol of γ-decalactone and 7.5 mmol of NaOH were mixed, and reacted at 60 °C for 2 h with magnetically stirring of 200 rpm. The reaction mixture was cooled down to room temperature. Then, 6.75 mmol of NBS was added, and the reaction was carried out at 40 °C with vigorous stirring (TLC tracking). Furthermore, the reaction mixture was cooled down to room temperature again, and adjusted the pH value to lower than 1.0 using 6.0 M sulfuric acid, and continued for 30 min. The reaction mixture was extracted with equal volume of ethyl acetate for three times, and the upper layer were isolated and combined, followed by drying over anhydrous Na_2SO_4. Then the organic solvent was evaporated under vacuum to obtain the crude product. Furthermore, crude product was purified by silica gel column to obtain 4-oxodecanoic acid. The purity of 4-oxodecanoic acid is 98.4 % after purification. Substrate 5-oxodecanoic acid was synthesized using the same method. The purity of 5-oxodecanoic acid is 99.0 % after purification.

Methyl 4-oxodecanoate (1 g) was synthesized by methyl esterification of 4-oxodecanoic acid with methanol. In 100 mL methanol, 4-oxodecanoic acid (10 g), 1 mL of 1 % concentrated sulfuric acid were mixed together. Anhydrous Na_2SO_4 (10 g) was added to remove the water produced by the reaction. Reaction was mechanically stirred at 200 rpm and, 70 °C, and refluxed for several hours. The progress of the reaction was monitored by TLC. The mobile phase ratio is petroleum ether: ethyl acetate = 4:1. After the reaction was completed, it was extracted with equal volume of ethyl acetate three times. The organic layers were isolated and combined, dried over anhydrous Na_2SO_4, and the crude product was obtained by rotary evaporation. Crude product was further purified by silica gel column to obtain 4-oxodecanoate methyl ester. The purity of 4-oxodecanoate methyl ester is 98.0 % after purification. Substrate 5-oxodecanoate methyl ester was synthesized employing the same method. The purity of 5-oxodecanoate methyl ester is 99.0 % after purification.

Other ketonates with different carbon chain lengths were synthesized by above method, and the purity was >95.0 % after purification.

2.3. Expression and purification of keto reductase

Genes encoding for keto reductases were synthesized by Tianlin Co. Ltd. (Shanghai, China). The target genes were inserted into the pET-28a (+) plasmid, and the recombinant plasmid was transformed into *E. coli* BL21 (DE3) and inoculated in 40 mL of LB medium (containing 50 mg/L kanamycin) for incubation at 37 °C and 180 rpm for 12 h. Expression of the target gene was induced by IPTG at a final concentration of 0.2 mM when OD_{600} was around 0.6, and then cultured at 16 °C for 12 h. The cells were collected by centrifugation, and the cells were suspended in PBS buffer (100 mM, pH 7.0) for sonication, followed by centrifugation at 8000 rpm for 20 min at 4 °C. The supernatant was collected and purified through a Ni-NTA column. After washed with solution A (100 mM PBS, pH 7.0, 20 mM imidazole), enzyme was eluted from solution B (100 mM PBS, pH 7.0, 200 mM imidazole). The enzyme activity was determined using 4-oxodecanoic acid as the substrate at 30 °C using the following method, and the purified enzyme solution was subjected to characterization.

2.4. Assay protocols of enzyme activity and stereoselectivity

The enzyme activity was determined by measuring the changes in OD_{340} of NADPH in a 96-well plate at 30 °C. The reaction mixture for activity consisted of 0.5 mM NADPH, 5 mM substrate, 100 mM PBS (pH 7.0) and appropriate amount of enzyme. One unit of enzyme activity (U) was defined as the amount of enzyme required to oxidize 1 μmol NADPH per minute under the above conditions. All activity was determined for at least three times.

A 1-mL reaction mixture containing 10 mM substrate, 5 U keto reductase crude enzyme extract, 20 mM glucose, 0.5 mM $NADP^+$, and 5 U GDHs crude enzyme extract in PBS buffer (pH 7.0, 100 mM), was employed for stereoselectivity analysis. The reaction was performed at 30 °C and 120 rpm for 12 h. After the reaction, 20 % sulfuric acid solution was added, and then heated at 90 °C for 2 h to complete the lactonization. Then, equal volume of ethyl acetate was added and subjected to vortex for product extraction. After centrifugation at 12000 rpm for 10 min, the upper organic phase was collected, and anhydrous Na_2SO_4 was added for drying overnight. After centrifugation at 12000 rpm for 10 min. Finally, the stereoselectivity of samples was analyzed by GC equipped with CP7502 column [19].

2.5. Characterization of purified HbKR

The pH-activity profile and optimal pH of *Hb*KR was investigated in pH 4–10 buffers containing 5 mM substrate and 0.5 mM NADPH at 30 °C. The temperature profile and optimal temperature were determined at 25–45 °C in PBS buffer (pH 7.0, 100 mM). Thermostability of *Hb*KR was determined by monitoring the residual activity of *Hb*KR at 30, 40, and 50 °C at different time intervals. The initial activity was regarded as 100 %. In addition, the residual activity of *Hb*KR was determined using standard enzyme activity assay protocol. All activity was determined for at least three times.

The effects of metal ions on activity of *Hb*KR and variants were investigated at 30 °C, including Ba^{2+}, K^+, Mg^{2+}, Na^+, Ca^{2+}, Zn^{2+}, Co^{2+}, Al^{3+}, Mn^{2+}, Fe^{3+}, and the concentration of metal ions was 1 mM. The organic solvent tolerance of *Hb*KR and variants was characterized by adding 5 % organic co-solvent in the activity assay system at 30 °C. The residual activities were measured using assay protocols as described in *2.4*. Control experiment was conducted without the addition of any additives, and was regarded as 100 %. All the experiment was performed in triplicate. Substrate specificity for reduction and oxidation activity of *Hb*KR and variants were investigated by employing assay protocols as described in *2.4*.

2.6. Kinetic parameters

Kinetic parameters were determined with different substrate concentrations (1.0–20 mM). The non-linear curve fitting method of Michaelis Menten equation was adopted to calculate the kinetic parameters.

2.7. Preparation process of chiral lactone

For GDH-coupled cofactor regeneration system, a 1-mL reaction mixture contained 1–10 $g{\cdot}L^{-1}$ purified *Hb*KR, double equivalent glucose, 2–5 $g{\cdot}L^{-1}$ purified GDH, 2 mM $NADP^+$, 5-oxodecanoic acid of different concentrations in PBS buffer (pH 7.0, 100 mM). For isopropanol (IPA)-coupled self-sufficient cofactor regeneration system, a 1-mL reaction mixture included 1–5 $g{\cdot}L^{-1}$ purified *Hb*KR, 2 mM $NADP^+$, 10 % IPA, 5-oxodecanoic acid of different concentrations in Tris-HCl (pH 8.5, 100 mM). The reactions were magnetically stirred at 30 °C for the synthesis of (*S*)-δ-decalactone.

For preparation of (*S*)-γ-decalactone, a 10-mL reaction mixture containing 20 mg/mL *Hb*KR enzyme powder, 20 mM glucose, 2 mM $NADP^+$, 10 mg/mL GDH enzyme powder, 5 mM 4-oxodecanoic acid in

PBS buffer (pH 7.0, 100 mM) was magnetically stirred. The reaction pH was maintained at 7.0 by titration with Na_2CO_3 (1.0 M). At different time intervals, samples of 100 μL were withdrawn from the reaction mixture. The reaction mixture was acidified with 20 % H_2SO_4 and heated for 2 h at 90 °C for intramolecular cyclization of the corresponding hydroxy acids, resulting in optically pure lactones. After extraction with ethyl acetate, the product was dried with anhydrous sodium sulfate, and analyzed by GC as describe above.

2.8. Site-directed mutagenesis of HbKR

Using recombinant plasmid pET28a-*Hb*KR as template, variants were obtained by PCR-based site-directed mutagenesis. The template in the resultant PCR product was removed by digestion with *Dpn*I. The digestive products are transformed into *E. coli* BL21(DE3).

2.9. Molecular docking and free energy decomposition analysis

The protein structure of *Hb*KR was predicted by AlphaFold2 (ID: AF-A0A1E4RM21-F1) [21] [22], and the structure model of *Hb*KR_{v2} was obtained accordingly. Molecular docking was performed using Discovery Studio. All docking calculations were accomplished with docking algorithms that took into account of ligand flexibility but maintain protein rigidity. *Hb*KR and *Hb*KR_{V2} were protonated by H++.

All the MD simulations were performed at the supercomputer center at School of Biotechnology using Amber20 packages with GPU acceleration. The force fields of substrate, protein and water were gaff, ff14SB and tip3p respectively. The systems were neutralized by adding chloride and sodium, and then TIP3P water box with a clearance distance of 15 Å were added around the proteins. Energy minimization of 5000 steps was conducted with the steepest descent method, followed by 1 ns heating at NVP from 0 K to 300 K, 1 ns equilibrating at NPT. MD was performed in NPV ensembles at 300 K for 20 ns with dt of 0.002 ps. All the simulations were performed for five times at least. The free energy decomposition analysis with MM-PB/GBSA were calculated with the Amber20.

3. Results and discussion

3.1. Screening of keto reductases

Initially, *carbonyl reductases* preserved in our laboratory were screened for enzymes with (*S*)-preference, and a carbonyl reductase (*Cp*AR2) from *Candida parapsilosis* was discovered. *Cp*AR2 exhibited specific activity of 0.3 $U{\cdot}mg^{-1}$ toward 5-oxodecanoic acid (**1f**), with stereoselectivity of 95 % (*S*). To explore novel carbonyl reductases with higher stereoselectivity toward **1f** and other long-chain keto acids/esters, the gene sequence of *Cp*AR2 was used as a probe for pBLAST sequence search in UniProt database. Five carbonyl reductases sharing 51–57 % sequence identity were selected (supplementary material **Table S1**). Although the activity of *Cp*AR2 for **1f** is higher than that of *Hb*KR, *Hb*KR showed excellent stereoselectivity of 99 % (*S*) toward 4-oxodecanoic acid (**1e**), 4-oxodecanoic acid methyl ester (**1g**), and **1f** (supplementary material **Fig. S3**). Therefore, *Hb*KR was selected for further study.

Multiple sequence alignment of *Hb*KR and several reported carbonyl reductases was performed. The primary sequence of *Hb*KR comprises 333 amino acids. The conserved motifs of *Hb*KR were also analyzed. The cofactor-binding motif in *Hb*KR, located between β1 and α1, consists of G8/A9/T10/G11/F12/I13/A14. The motif D233/V234/R235/D236 between β9 and α8, is conserved for stabilizing the adenine ring of NADPH. The catalytic triad of *Hb*KR locates in the regions of α5 and α6. It can be seen that all the conserved motifs of *Hb*KR are consistent with the characteristics of extended SDR subfamily (supplementary material **Fig. S1**).

3.2. Characterization of HbKR

The enzyme properties of purified *Hb*KR was characterized. Based on SDS-PAGE analysis, purified *Hb*KR migrated at around 37.15 kDa, which is in consistent with its theoretical molecular weight (supplementary material **Fig. S2**). The specific activity of the purified *Hb*KR was determined to be 0.86 $U{\cdot}mg^{-1}$ for **1f**.

Effects of pH and temperature on the activity and stability of *Hb*KR were explored (Fig. 1). The reduction and oxidation activities were examined with **1f** and isopropanol (IPA) as substrates, respectively. *Hb*KR displayed the highest reduction activity at pH 6.0 in PBS buffers. Relative activities at pH 6.0 were determined to be 32.2 % of the highest activity in sodium citrate buffer. The reduction activity decreased sharply in buffers with pH values higher than 6.0 or lower than 6.0 (Fig. 1A). The optimum pH for oxidation reaction was determined to be pH 9.0 (Fig. 1B). The oxidation activity decreased quickly in buffers with pH values higher than 9.0 or lower than 9.0. The narrow pH range indicates that the pH of reaction could significantly affect the protonation or deprotonation activity of catalytic residues Tyr160, therefore influence enzyme activities.

The relative activity of *Hb*KR was investigated over a temperature ranging from 20 to 45 °C (Fig. 1C). The activity of *Hb*KR gradually increased from 20 to 30 °C and reached the maximum at 30 °C. A further increase in the temperature resulted in a steep decrease in the activity. For investigate the thermostability analysis, the half-lives ($t_{1/2}$) of *Hb*KR were determined by incubating at 30, 40, and 50 °C (Fig. 1D). *Hb*KR was inactivated immediately after incubation at 50 °C for merely 5 min. After incubation at 40 °C for 0.5 h, *Hb*KR could retain only about 5.2 % of the initial activity. The $t_{1/2}$ value of *Hb*KR was calculated to be 24 h at 30 °C according to the Arrhenius deactivation equation. Above results indicates that *Hb*KR is a mesophilic enzyme.

Influence of metal ions and chemical reagents on the activity of *Hb*KR was also explored (Table 1). The activity of *Hb*KR increased slightly in the presence of 1 mM K^+, Mg^{2+}, Ca^{2+}, Ba^{2+} and Na^+. Interestingly, the activity was activated by Ba^{2+} by around 28 %. The activity of *Hb*KR was severely inhibited by Zn^{2+}, Co^{2+}, Al^{3+} and Mn^{2+}, especially Zn^{2+}, leading to a relative activity of 28.8 %. Influence of several organic co-solvents was also investigated. Several solvents, such as DMSO, methanol and acetone, had little effect on the activity of *Hb*KR, indicating its potential application as co-solvent in biocatalytic reactions.

3.3. Tailor-made engineering of HbKR

According to protein structure predicted by AlphaFold2, protein engineering of *Hb*KR was conducted to improve its catalytic activity while maintaining excellent stereoselectivity. In order to improve the activity of *Hb*KR against large steric hindrance substrates and maintain excellent stereoselectivity, 5-Oxodecanoic acid (**1f**) was selected as the model substrate, and docked into the active center of *Hb*KR. Although the substrate **1f** could be accommodated in the substrate binding pocket of *Hb*KR, it was structurally bended and located far away from the catalytic Tyr160 (3.5 Å) which is not favorable for efficient catalysis (Fig. 4A).

In order to expand the substrate-binding pocket and enhance interaction between the keto acid substrate and surrounding residues, thirty-one residues within 12 Å surrounding the reactive hydroxyl group of Y160 were selected for mutagenesis with alanine and positively charged amino acid scanning, excluding amino acids that interacted with cofactor and non-steric amino acids (supplementary material **Fig. S3**). As can be seen in Fig. 2, for alanine scanning, most variants showed similar or seriously compromised activity and stereoselectivity compared with *Hb*KR. Remarkably, variant F207A (*Hb*KR_{V1}) with 6.3 times increased specific activity. For positively charged amino acid scanning, the highest enzyme activity was achieved with variant F86H, showed 1.4 times increased activity. To explore the influence of site F207 and F86, saturation mutagenesis of F207 and F86 were performed,

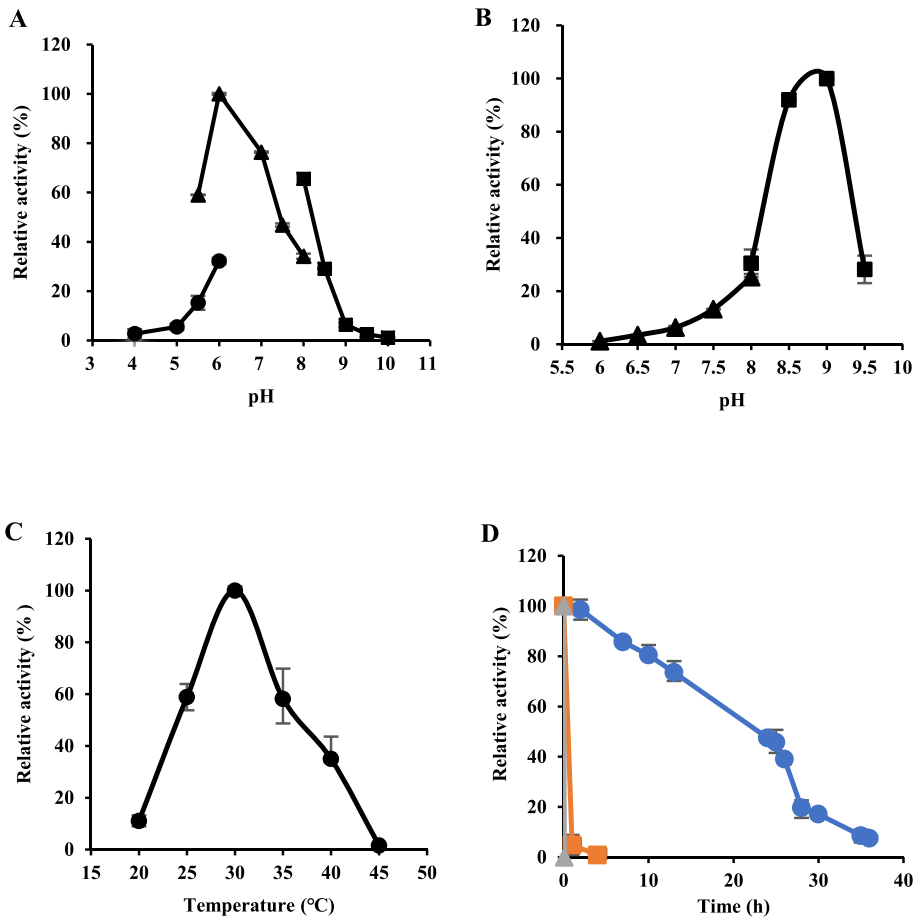

Fig. 1. (A) Effect of pH on reduction activity of *Hb*KR; (B) Effect of pH on oxidation activity of *Hb*KR; (C) Effect of temperature on reduction activity of *Hb*KR; (D) Thermostability of *Hb*KR at 30 °C (blue), 40 °C (orange), and 50 °C (gray). Effect of pH was performed in following 100 mM buffers: (●) sodium citrate (pH 4.0–6.0), (▲) phosphate (pH 5.5–8.0), (■) Glycine-NaOH (pH 8.0–10.0).

Table 1
Effects of various metal ions and chemical reagents on the activity of *Hb*KR.

Metal ion [1 mM]	Relative activity (%)	Chemical reagent [5 % (v/v)]	Relative activity (%)
Control	100.0 ± 2.2	Ethanol	63.0 ± 4.0
K^+	126.0 ± 3.7	Methanol	82.0 ± 0.2
Mg^{2+}	117.0 ± 3.2	Isopropanol	62.8 ± 1.2
Zn^{2+}	28.8 ± 0.1	DMSO	93.6 ± 0.2
Co^{2+}	35.1 ± 1.2	Acetonitrile	44.9 ± 0.1
Ca^{2+}	104.3 ± 2.9	2,3-Butanediol	34.7 ± 0.4
Ba^{2+}	128.0 ± 5.3	Acetone	78.0 ± 0.8
Al^{3+}	30.6 ± 3.6		
Mn^{2+}	36.4 ± 3.7		
Na^+	107.2 ± 0.6		

All the measurements were performed in triplicate. Data are presented as average ± standard deviation.

in which F207A and F86E were the best variant respectively (Fig. 3). Using F207A as the template, iterative saturation mutagenesis was performed at F86. Beneficial variant F207A/F86M (*Hb*KR_{V2}) was achieved with 9.7 times increased activity (Fig. 3), and the stereoselectivity of *Hb*KR_{V1} and *Hb*KR_{V2} for **1f** and **1e** is both 99 % (*S*) (supplementary material **Fig. S3**).

3.4. Kinetic parameters of HbKR and variants

Kinetic parameters of *Hb*KR and variants were determined using **1f** as the substrate to understand the effect of substrate binding on their

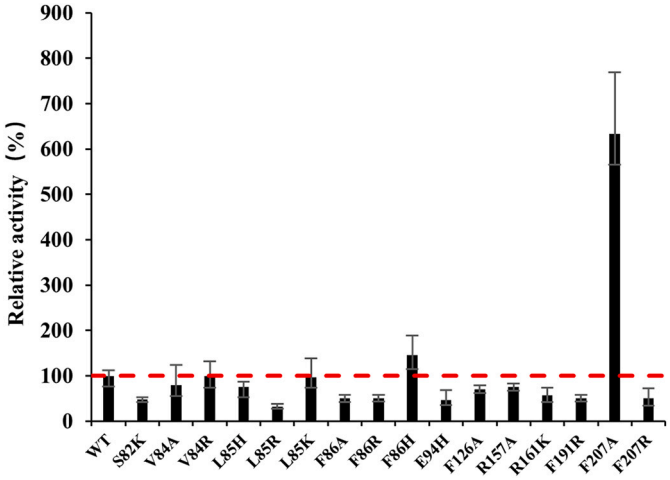

Fig. 2. Relative activity of *Hb*KR WT and variants toward 5-oxodecanoic acid for alanine scanning and positively charged amino acid scanning.

catalytic performance. As shown in Table 2, the catalytic efficiency (k_{cat}/K_M) of *Hb*KR_{V1} was improved by 15.2 times, owing to the reduced K_M and increased k_{cat} values. For *Hb*KR_{V2}, both K_M and k_{cat} values were higher than *Hb*KR_{V1}, leading to a 17.9- fold enhanced catalytic efficiency, ascribing to the significant increase in k_{cat}. Consequently, the catalytic properties of *Hb*KR were significantly improved after

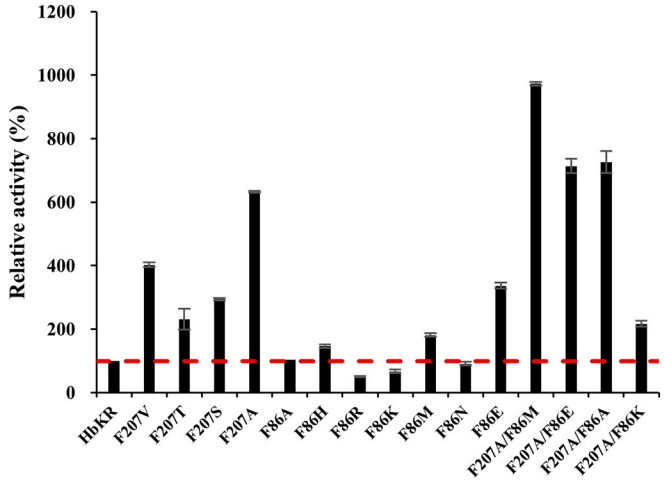

Fig. 3. Relative activity of single/double variants of F207 and F86.

structural-guided protein engineering.

3.5. Reduction/oxidation activity and substrate specificity of HbKR and variants

The catalytic properties of *Hb*KR and variants toward 12 keto acid/ester substrates were investigated. As shown in Table 3, *Hb*KR could catalyze the reduction of all the tested ketones, especially 5-oxooctanoic acid (**1b**), methyl 5-oxohexanoate (**1d**), **1f**, and 5-oxododecanoic acid (**1j**). Moreover, the reduction activity of *Hb*KR was dramatically affected by the position of carbonyl group. Overall, *Hb*KR showed higher activity toward δ-keto acids/esters than that of γ-keto acids/esters, indicating it favors δ-keto acid/ester substrates. Surprisingly, *Hb*KR has a relatively high specific activity of 1.33 U·mg^{-1} for **1j** and 0.27 U·mg^{-1} for 4-oxododecanoic acid (**1i**), demonstrating its high catalytic activity toward long-chain keto acid/esters substrates. For *Hb*KR, the highest activity of 2.84 U·mg^{-1} was determined with **1b**. *Hb*KR$_{V2}$ showed specific activity of reaches 6.6 U·mg^{-1} toward **1j**, 5 times higher than that of *Hb*KR. Differently, *Hb*KR$_{V2}$ displayed the highest specific activity of 8.37 U·mg^{-1} toward **1f**, representing a 9.7-fold increase than that of *Hb*KR (0.86 U·mg^{-1}). Moreover, *Hb*KR$_{V2}$ showed improved activity of 2.14 U·mg^{-1} for 4-oxodecanoic acid (**1e**). The result indicates that the tailor-made protein engineering of *Hb*KR is effective, and is more favorable for the synthesis of (*S*)-γ-decalactone and (*S*)-δ-decalactone. In particular, the substrate preference of *Hb*KR is different from that of *Sm*CR, indicating it has a unique catalytic mechanism.

In addition to the reduction reaction, the oxidation activity of *Hb*KR and variants was also investigated (Table 3). Different types of alcohols were selected for the characterization of substrate specificity, including saturated alcohols, diols, cyclic alcohols, and aromatic alcohols. For *Hb*KR, the highest activity of 2.43 U·mg^{-1} was determined with (*S*)-phenylethanol among various alcohols, while it showed no detectable activity for (*R*)-phenylethanol. This result indicates that *Hb*KR could have an excellent stereoselectivity in the oxidative resolution of racemic phenylethanol. Additionally, *Hb*KR showed higher activity toward larger substrates such as 3-methylcyclohexanol and 2-butyl alcohol, whereas lower activity for smaller substrates such as n-propanol. Therefore, *Hb*KR preferably catalyzes the oxidation of aromatic and cyclic alcohol substrates. Compared with *Hb*KR, the oxidation activity of *Hb*KR$_{V2}$ was significantly lower. Notably, *Hb*KR$_{V2}$ also demonstrated a higher oxidative activity for (*S*)-phenylethanol than (*R*)-phenylethanol, suggesting that it maintained the same stereoselectivity in oxidation of racemic phenylethanol.

3.6. Asymmetric synthesis of (S)-decalactone catalyzed by HbKR and variants

The asymmetric reduction catalyzed by *Hb*KR and variants was conducted (Table 4). Here, both glucose dehydrogenase (GDH)-coupled and isopropanol (IPA)-coupled self-sufficient cofactor recycling systems were explored. In GDH-coupled system, a final conversion ratio of 91 % with 99 % (*S*) was reached by *Hb*KR at 10 mM **1f**. For *Hb*KR$_{V1}$ and *Hb*KR$_{V2}$, 10 mM **1f** was converted completely with 99 % (*S*) after 1 h. At 50 mM **1f**, final conversion ratios of 63.6 %, 94.9 % and 95.4 % were reached by *Hb*KR, *Hb*KR$_{V1}$ and *Hb*KR$_{V2}$ respectively after 1 h. Notably, both variants showed significantly higher conversion ratio than that of *Hb*KR, indicating their enhanced catalytic efficiency, while maintaining excellent stereoselectivity. At a further enhanced 100 mM **1f**, a slightly decrease conversion ratio of 90.4 % was achieved by *Hb*KR$_{V2}$.

In GDH-coupled system, sodium gluconate is produced as a by-product. Also, co-solvents should be added to promote solubility of substrates. Based on the oxidation activity of *Hb*KR, a IPA-coupled self-sufficient cofactor system was developed, in which IPA serves both as hydrogen donor and co-solvent (Table 4). For *Hb*KR, 10 mM **1f** was converted with 89.0 % conversion ratio and 99 % *e.e.* (*S*). For *Hb*KR$_{V1}$ and *Hb*KR$_{V2}$, a complete conversion was reached at 10 mM **1f** in 1 h. At 50 mM **1f**, however, compromised conversion ratios of 81.4 % and 72.5 % was observed with *Hb*KR$_{V1}$ and *Hb*KR$_{V2}$ respectively. The decreased conversion ratio of *Hb*KR$_{V2}$ may be related to its decreased oxidation activity toward IPA (Table 3). This result indicates that cofactor recycling through IPA is feasible for the asymmetric reduction catalyzed by *Hb*KR and variants, and further optimization of reaction system is required to improve the conversion at higher substrate concentrations. In addition, (*S*)-γ-decalactone was also synthesized with **1e** as substrate. In a 10-mL reaction system with GDH-coupled NADPH recycle, 92 % of 10 mM **1e** was converted in 99 % *e.e.* (*S*) within 1 h.

3.7. Molecular docking of HbKR and variants

To explore the catalytic mechanism of *Hb*KR, molecular docking analysis was conducted using **1f** and 5-oxodecanoic acid methyl ester (**1h**) as substrates. The structural model of variant *Hb*KR$_{V2}$ was also predicted by AlphaFold2. As shown in Fig. 4A–D, **1f** and **1h** were situated in the active center of *Hb*KR and *Hb*KR$_{V2}$ with the carbonyl group pointing toward the catalytic Y160 and the carbonyl C atom in a pro-productive state for hydride transfer from NADPH. According to the Prelog priority, the transferring of hydride in the *re*-face will result in *pro-S* conformation and produce (*S*)-alcohol [23].

In *Hb*KR, the presence of larger F86 and F207 prevents substrates from penetrating into the binding pocket. Hence, substrate **1f** and **1h**

Table 2
Specific activity and kinetic parameters of *Hb*KR and variants toward **1f**.

Enzyme	Mutation	Specific activity (U/mg)	K_M (mmol·L^{-1})	V_{max} (μmol·min^{-1}·mg^{-1})	k_{cat} (s^{-1})	k_{cat}/K_M (s^{-1}•mM^{-1})	Fold[a]
*Hb*KR	–	0.86	3.78 ± 0.2	1.88 ± 0.05	1.16 ± 0.3	0.31 ± 0.02	1.0
*Hb*KR$_{V1}$	F207A	5.38	0.58 ± 0.11	4.42 ± 0.28	2.73 ± 0.17	4.71 ± 1.24	15.2
*Hb*KR$_{V2}$	F207A/F86M	8.37	0.95 ± 0.22	8.53 ± 0.82	5.26 ± 0.51	5.54 ± 1.94	17.9

All the measurements were performed in triplicate. Data are presented as average ± standard deviation.
[a] Fold change enhancement in k_{cat}/K_M compared with *Hb*KR.

Table 3
Specific activity of *Hb*KR and variants toward keto acids/esters and alcohols.

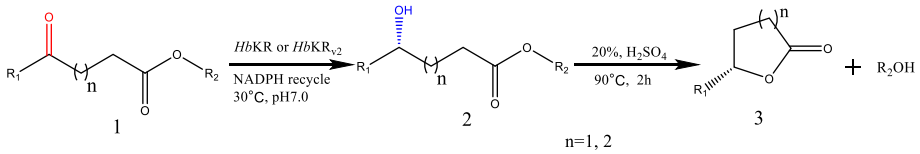

n=1, 2
R_1=C_3H_7, C_4H_9, C_5H_{11}, C_6H_{13},C_7H_{15}, C_8H_{17}
R_2=H, CH_3

Substrate		n	R_1	R_2	Specific activity (U/mg)		
					*Hb*KR	*Hb*KR$_{V2}$	Fold[c]
Ketones [a]	4-oxooctanoic acid (**1a**)	1	C_4H_9	H	0.19	1.25	6.5
	5-oxooctanoic acid (**1b**)	2	C_3H_7	H	1.24	2.25	1.8
	4-oxooctanoic acid methyl ester (**1c**)	1	C_4H_9	CH_3	0.17	1.68	9.8
	5-oxooctanoic acid methyl ester (**1d**)	2	C_3H_7	CH_3	2.84	3.37	1.2
	4-oxodecanoic acid (**1e**)	1	C_6H_{13}	H	0.34	2.14	6.2
	5-oxodecanoic acid (**1f**)	2	C_5H_{11}	H	0.86	8.37	9.7
	4-oxodecanoic acid methyl ester (**1g**)	1	C_6H_{13}	CH_3	0.13	1.40	10.6
	5-oxodecanoic acid methyl ester (**1h**)	2	C_5H_{11}	CH_3	0.45	4.34	9.6
	4-oxdodecanoic acid (**1i**)	1	C_8H_{17}	H	0.27	1.41	5.1
	5-oxdodecanoic acid (**1j**)	2	C_7H_{15}	H	1.33	6.60	5.0
	4-oxdodecanoic acid methyl ester (**1k**)	1	C_8H_{17}	CH_3	0.04	0.12	2.6
	5-oxdodecanoic acid methyl ester (**1l**)	2	C_7H_{15}	CH_3	0.09	0.79	8.8
Alcohols[b]	*R*-phenylethanol	–	–	–	0.01	*ND*[d]	*NA*[e]
	S-phenylethanol	–	–	–	2.43	0.052	46.7
	n-propanol	–	–	–	0.09	0.009	10
	isopropanol	–	–	–	1.09	0.046	23.7
	2-butyl alcohol	–	–	–	0.83	0.027	30.7
	3-methylcyclohexanol	–	–	–	1.45	0.003	483
	4-ethylcyclohexanol	–	–	–	0.28	0.009	31.1
	2,3-butanediol	–	–	–	0.45	*ND*	*NA*

[a] Specific activity was determined in sodium phosphate buffer (100 mM, pH 7.0) containing 5 mM ketone substrate, 1 mM NADPH, and appropriate amount of purified enzymes at 30 °C.
[b] Specific activity was determined in sodium phosphate buffer (100 mM, pH 8.0) containing 5 mM alcohol substrate, 1 mM NADPH, and appropriate amount of purified enzymes at 30 °C.
[c] Fold change in the activity of *Hb*KR$_{V2}$ vs *Hb*KR.
[d] *ND*: not activity was detected.
[e] *NA*: not available.

Table 4
Biocatalytic conversion of **1f** by *Hb*KR and variants with GDH-coupled and IPA-coupled self-sufficient cofactor regeneration systems.

	1f (mM)	*Hb*KR (g·L^{-1})	GDH[a] (g·L^{-1})	IPA [b] (%)	NADP$^+$ (mM)	Conversion (%)	*e.e.* (%, *S*)
*Hb*KR	10	1	2	–	0.2	91.0	99
	10	1	–	10	0.2	89.0	99
	50	5	5	–	0.5	63.6	99
*Hb*KR$_{V1}$	10	1	2	–	0.2	100	99
	10	1	–	10	0.2	100	99
	50	5	5	–	0.5	94.9	99
	50	5	–	10	0.5	81.4	99
*Hb*KR$_{V2}$	10	1	2	–	0.2	100	99
	10	1	–	10	0.2	100	99
	50	5	5	–	0.5	95.4	99
	50	5	–	10	0.5	72.5	99
	100	10	5	–	0.5	90.4	99

For 10 mM 1f, 0.2 mM NADP+ and 2 g/L GDH were added.
For 50 mM and 100 mM 1f, 0.5 mM NADP+ and 5 g/L GDH were added.
For all the reactions, reaction temperature was 30 °C and reaction time was 1 h.
[a] GDH-coupled cofactor regeneration: 1 mL reaction system in PBS buffer (100 mM, pH 7.0).
[b] IPA-coupled self-sufficient cofactor regeneration: 1 mL reaction system in Tris-HCl buffer (100 mM, pH 8.5).

have to bend by about 90° to access the catalytic Y160. Extra interactions such as the unfavorable interaction between R157 and the hydrophobic terminal of **1f** will force the substrate to bend and is conducive for the formation of *pro-S* conformation (Fig. 4A, B).

In *Hb*KR$_{V2}$, mutation of F86 and F207 into smaller Met and Ala eliminates the steric hindrance effect, and leads to an enlarged volume of about 40 Å^3 for substrate binding pocket compared with *Hb*KR. This change is especially beneficial for the entry of long chain substrates into the substrate binding pocket. The distance between **1f** and Y160 was reduced from 3.5 Å to 2.6 Å in *Hb*KR$_{V2}$, which is advantageous for

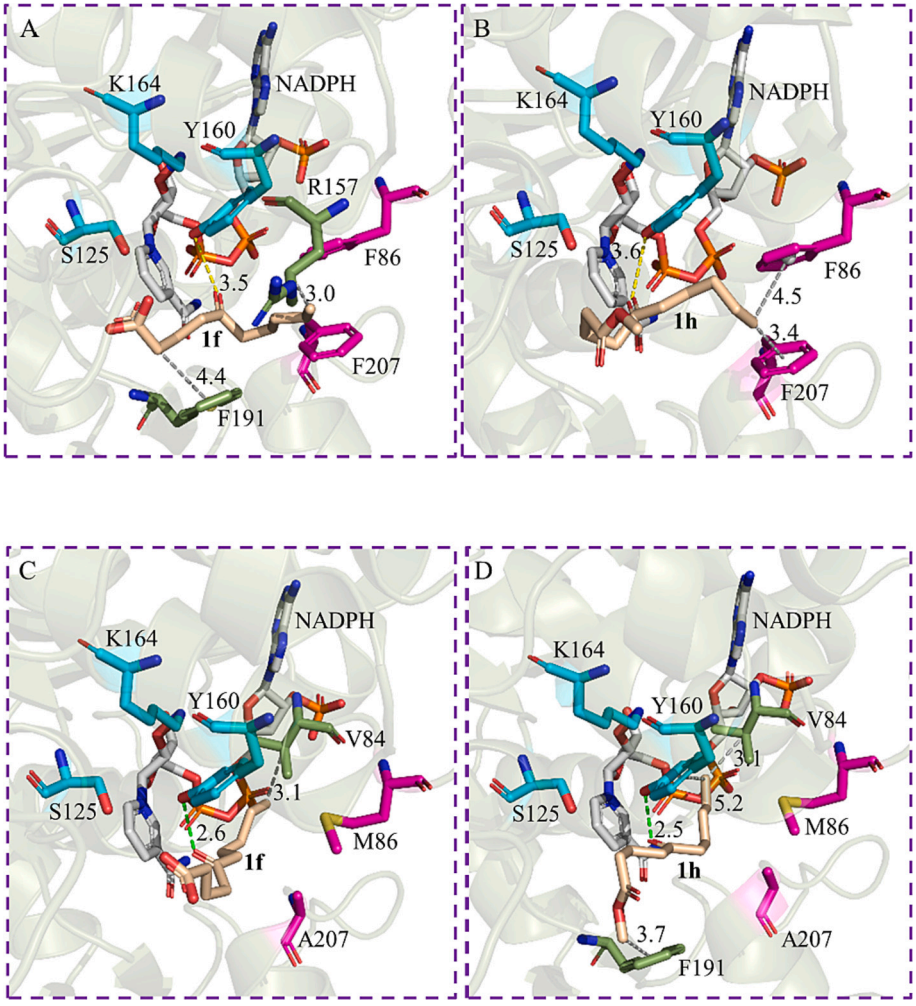

Fig. 4. Interaction analysis between substrates **1f**, **1h** and *Hb*KR, *Hb*KR$_{V2}$. (A) **1f** and *Hb*KR, (B) **1h** and *Hb*KR, (C) **1f** and *Hb*KR$_{V2}$, (D) **1f** and *Hb*KR$_{V2}$. Gray: NADPH; cyan: catalytic triad Y160/K164/S125; wheat: **1f** and **1h**; purple: mutation sites; green: residues with hydrophobic interactions.

nucleophilic attack from Y160, accounting for the significantly increased catalytic efficiency of *Hb*KR$_{V2}$. Moreover, more interactions were also observed, such as hydrophobic interactions between V84 and the hydrophobic end of **1f** and **1h** in *Hb*KR$_{V2}$, which also contribute to the stabilization of the *pro-S* conformation of substrates and formation of (*S*)-alcohols (Fig. 4C, D).

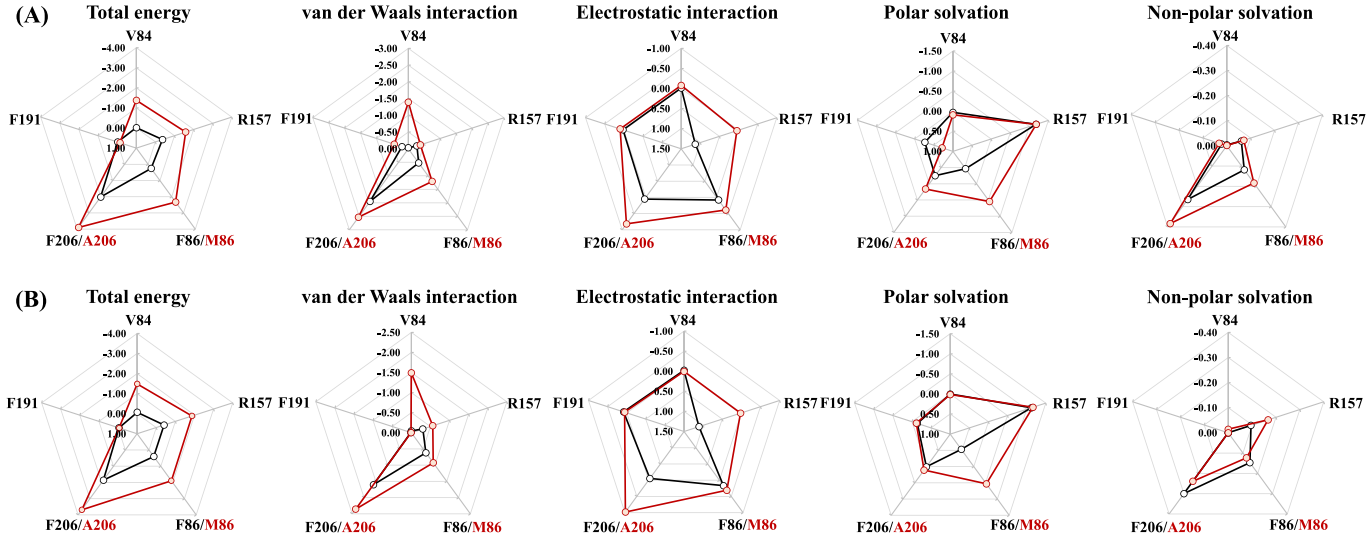

Fig. 5. Per-residue free energy decomposition of *Hb*KR and *Hb*KR$_{V2}$ toward **1f** (A) and **1h** (B) employing MMPB/GBSA. Black dot and line: *Hb*KR, red dot and line: *Hb*KR$_{V2}$. Energy was given in kcal·mol^{-1}.

Free energy decomposition analysis was performed using MMPB/GBSA from MD simulations. As shown in Fig. 5, V84, R159, M86 and A207 in *Hb*KR$_{V2}$ displayed lower total energies and provided favorable interactions for the binding of **1f** and **1h**. In *Hb*KR$_{V2}$, mutation of F86 into M86 released enough volume for the hydrophobic terminal of **1f** and **1h** with V84, resulting in significantly increased van der Waals interactions of –1.39 and –1.49 kcal·mol^{-1} respectively, much higher than –0.03 and –0.05 kcal·mol^{-1} in *Hb*KR. In *Hb*KR, the total energy of R159 toward **1f** was −0.05 kcal·mol^{-1}, which was mainly caused by the unfavorable electrostatic interaction of 1.13 kcal·mol^{-1} between R159 and hydrophobic terminal of **1f**. While in *Hb*KR$_{V2}$, R159 became favorable with total energy of −1.58 kcal·mol$^{-1,}$ because of the elimination of unfavorable electrostatic interaction (Fig. 5A). Compared with F86 and F207, M86 and A207 in *Hb*KR$_{V2}$ displayed increased van der Waal interactions toward **1f** and **1h**. Moreover, A207 exhibited stronger electrostatic interactions toward substrates. All above provided deep molecular insights into the enhanced catalytic efficiency of *Hb*KR$_{V2}$.

4. Conclusions

A novel keto reductase *Hb*KR with both reduction and oxidation activity was discovered from *Hyphopichia burtoni* by gene mining. *Hb*KR has excellent stereoselectivity for long chain keto acids/esters, especially 5-oxodecanoic acid and 4-oxodecanoic acid. By expanding the volume of substrate binding pocket, a beneficial variant F207A/F86M (*Hb*KR$_{V2}$) was obtained with 17.9-fold improved catalytic efficiency against **1f**. Catalyzed by *Hb*KR$_{V2}$, (*S*)-*δ*-decalactone was synthesized at 100 mM **1f**. Interestingly, the asymmetric reduction system with IPA-coupled self-sufficient cofactor regeneration could be operated based on dual-function *Hb*KR with reduction and oxidation activity. In summary, a novel and efficient enzymatic approach was developed for the synthesis of (*S*)-*γ*- and (*S*)-*δ*-lactones with excellent stereoselectivity. In future work, the thermostability of *Hb*KR for should be further engineered for potential industrial applications.

Ethical statement

This article does not contain any studies with human participants or animals performed by any of the authors.

CRediT authorship contribution statement

Shuo Wang: Writing – original draft, Validation, Investigation, Data curation. **Guochao Xu:** Writing – original draft, Supervision, Methodology, Funding acquisition, Conceptualization. **Ye Ni:** Writing – review & editing, Supervision, Funding acquisition, Conceptualization.

Declaration of competing interest

The authors declare that they have no known competing financial interests or personal relationships that could have appeared to influence the work reported in this paper.

Data availability

All data generated or analyzed during this study are included in this published article and its supplementary information files.

Acknowledgements

We are grateful to the National Key Research and Development Program (2021YFC2102700), National Natural Science Foundation of China (22377040, 22378169) for the financial support of this research.

Appendix A. Supplementary data

Supplementary data to this article can be found online at https://doi.org/10.1016/j.ijbiomac.2024.129870.

References

[1] K. Aplander, O. Hidestål, K. Katebzadeh, U.M. Lindström, A green and facile route to γ- and δ-lactones via efficient Pinner-cyclization of hydroxynitriles in water, Green Chem. 8 (1) (2006) 22–24. https://doi.org/10.1039/B513656C.
[2] E. Brenna, C. Fuganti, F.G. Gatti, S. Serra, Biocatalytic methods for the synthesis of enantioenriched odor active compounds, Chem. Rev. 111 (7) (2011) 4036–4072, https://doi.org/10.1021/cr100289r.
[3] R. Bentley, The nose as a stereochemist. Enantiomers and odor, Chem. Rev. 106 (9) (2006) 4099–4112, https://doi.org/10.1021/cr050049t.
[4] J.S. Kandula, V.P.K. Rayala, R. Pullapanthula, Chirality: an inescapable concept for the pharmaceutical, bio-pharmaceutical, food, and cosmetic industries, Separ. Sci. Plus 6 (4) (2023), https://doi.org/10.1002/sscp.202200131.
[5] F. Boratynski, K. Dancewicz, M. Paprocka, B. Gabrys, C. Wawrzenczyk, Chemo-enzymatic synthesis of optically active γ- and δ-Decalactones and their effect on aphid probing, feeding and settling behavior, PLoS One 11 (1) (2016), https://doi.org/10.1371/journal.pone.0146160.
[6] J. Manning, M. Tavanti, J.L. orter, N. Kress, S.P. De Visser, N.J. Turner, S.L. Flitsch, Regio- and enantio-selective chemo-enzymatic C-H-Lactonization of decanoic acid to (S)-delta-Decalactone, Angew. Chem. Int. Ed. Eng. 58 (17) (2019) 5668–5671, https://doi.org/10.1002/anie.201901242.
[7] A. Braga, I. Belo, Biotechnological production of γ-decalactone, a peach like aroma, by Yarrowia lipolytica, World J. Microbiol. Biotechnol. 32 (10) (2016), https://doi.org/10.1007/s11274-016-2116-2.
[8] J.C. Zhu, X.Y. Cao, Y.W. Niu, Z.B. Xiao, Investigation of lactone chiral enantiomers and their contribution to the aroma of Longjing tea by odor activity value and S-curve, J. Agric. Food Chem. 71 (17) (2023) 6691–6698, https://doi.org/10.1021/acs.jafc.3c00860.
[9] P. Naknean, M. Meenune, Factors affecting retention and release of flavour compounds in food carbohydrates, Int. Food Res. J. 17 (1) (2010) 23–34. http://ifrj.upm.edu.my/17%20(01)%202010/(3)%20IFRJ-2010-23-34%20Mutita%20Thailand.pdf.
[10] S. Tamogami, K. Awano, T. Kitahara, Analysis of the enantiomeric ratios of chiral components in absolute jasmine, Flavour Fragr. J. 16 (3) (2001) 161–163, https://doi.org/10.1002/ffj.969.
[11] P. Staniatopoulos, E. Brohan, C. Prevost, T.E. Siebert, M. Herderich, P. Darriet, Influence of chirality of lactones on the perception of some typical fruity notes through perceptual interaction phenomena in Bordeaux dessert wines, J. Agric. Food Chem. 64 (43) (2016) 8160–8167, https://doi.org/10.1021/acs.jafc.6b03117.
[12] F. Boratynski, K. Dancewicz, M. Paprocka, B. Gabrys, C. Wawrzenczyk, Chemo-enzymatic synthesis of optically active gamma- and delta-decalactones and their effect on aphid probing, feeding and settling behavior, PLoS One 11 (1) (2016), https://doi.org/10.1371/journal.pone.0146160.
[13] N. Arai, T. Namba, K. Kawaguchi, Y. Matsumoto, T. Ohkuma, Chemoselectivity control in the asymmetric hydrogenation of γ- and δ-keto esters into hydroxy esters or diols, Ang. Chem.-Int. Ed. 57 (5) (2018) 1386–1389, https://doi.org/10.1002/anie.201711363.
[14] S. Meninno, C. Volpe, A. Lattanzi, One-pot quinine-catalyzed synthesis of α-chiral γ-keto esters: enantioenriched precursors of cis α,γ-substituted-γ-butyrolactones, Adv. Synth. Catal. 358 (17) (2016) 2845–2848, https://doi.org/10.1002/adsc.201600427.
[15] O. Pàmies, J.E. Bäckvall, Enzymatic kinetic resolution and chemoenzymatic dynamic kinetic resolution of δ-hydroxy esters.: an efficient route to chiral δ-lactones, J. Organomet. Chem. 67 (4) (2002) 1261–1265, https://doi.org/10.1021/jo016096c.
[16] E.M.M. Abdelraheem, H. Busch, U. Hanefeld, F. Tonin, Biocatalysis explained: from pharmaceutical to bulk chemical production, React. Chem. Eng. 4 (11) (2019) 1878–1894. https://doi.org/10.1039/C9RE00301K.
[17] L. Chu, X. Zhang, J. Li, X. Deng, M. Wu, Y. Cheng, W. Zhu, X. Qian, Y. Bai, Continuous-flow synthesis of polysubstituted γ-butyrolactones via enzymatic cascade catalysis, Chin. Chem. Lett. (2023) 108896, https://doi.org/10.1016/j.cclet.2023.108896.
[18] C. Zhang, J. Pan, C.-X. Li, Y.-P. Bai, J.-H. Xu, Asymmetric bioreduction of keto groups of 4- and 5-Oxodecanoic acids/esters with a new carbonyl reductase, Catal. Commun. 102 (2017) 35–39, https://doi.org/10.1016/j.catcom.2017.08.023.
[19] M. Chen, X.Y. Zhang, C.G. Xing, C. Zhang, Y.C. Zheng, J. Pan, J.H. Xu, Y.P. Bai, Efficient stereoselective synthesis of structurally diverse γ- and δ-lactones using an engineered carbonyl reductase, ChemCatChem 11 (11) (2019) 2600–2606, https://doi.org/10.1002/cctc.201900382.
[20] F.F. Özgen, A. Jorea, L. Capaldo, R. Kourist, D. Ravelli, S. Schmidt, The synthesis of chiral γ-lactones by merging decatungstate photocatalysis with biocatalysis, Chemcatchem 14 (19) (2022), https://doi.org/10.1002/cctc.202200855.
[21] J. Jumper, R. Evans, A. Pritzel, T. Green, M. Figurnov, O. Ronneberger, K. Tunyasuvunakool, R. Bates, A. Zídek, A. Potapenko, A. Bridgland, C. Meyer, S.A. A. Kohl, A.J. Ballard, A. Cowie, B. Romera-Paredes, S. Nikolov, R. Jain, J. Adler, T. Back, S. Petersen, D. Reiman, E. Clancy, M. Zielinski, M. Steinegger, M. Pacholska, T. Berghammer, S. Bodenstein, D. Silver, O. Vinyals, A.W. Senior, K. Kavukcuoglu, P. Kohli, D. Hassabis, Highly accurate protein structure prediction

with AlphaFold, Nature 596 (7873) (2021), https://doi.org/10.1038/s41586-021-03819-2 (583-+).
[22] M. Varadi, S. Anyango, M. Deshpande, S. Nair, C. Natassia, G. Yordanova, D. Yuan, O. Stroe, G. Wood, A. Laydon, A. Zídek, T. Green, K. Tunyasuvunakool, S. Petersen, J. Jumper, E. Clancy, R. Green, A. Vora, M. Lutfi, M. Figurnov, A. Cowie, N. Hobbs, P. Kohli, G. Kleywegt, E. Birney, D. Hassabis, S. Velankar, AlphaFold Protein Structure Database: massively expanding the structural coverage of protein-sequence space with high-accuracy models, Nucleic Acids Res. 50 (D1) (2022) D439–D444, https://doi.org/10.1093/nar/gkab1061.
[23] J.C. Zhang, J.Y. Zhou, G.C. Xu, Y. Ni, Stereodivergent evolution of KpADH for the asymmetric reduction of diaryl ketones with para-substituents, Mol. Catal. 524 (2022), https://doi.org/10.1016/j.mcat.2022.112315.